Journal of Computational Physics **176,** 129–144 (2002)
doi:10.1006/jcph.2001.6971, available online at http://www.idealibrary.com on IDEAL®

Numerical Analysis of Dusty-Gas Flows

T. Saito

Shock Wave Research Center, Institute of Fluid Science, Tohoku University,
2-1-1 Katahira, Aoba-ku, Sendai, 980-8577 Japan
E-mail: saito@bellanca.ifs.tohoku.ac.jp

Received December 19, 2000; revised September 14, 2001

This paper presents the development of a numerical code for simulating unsteady dusty-gas flows including shock and rarefaction waves. The numerical results obtained for a shock tube problem are used for validating the accuracy and performance of the code. The code is then extended for simulating two-dimensional problems. Since the interactions between the gas and particle phases are calculated with the operator splitting technique, we can choose numerical schemes independently for the different phases. A semi-analytical method is developed for the dust phase, while the TVD scheme of Harten and Yee is chosen for the gas phase. Throughout this study, computations are carried out on SGI Origin2000, a parallel computer with multiple of RISC based processors. The efficient use of the parallel computer system is an important issue and the code implementation on Origin2000 is also described. Flow profiles of both the gas and solid particles behind the steady shock wave are calculated by integrating the steady conservation equations. The good agreement between the pseudo-stationary solutions and those from the current numerical code validates the numerical approach and the actual coding. The pseudo-stationary shock profiles can also be used as initial conditions of unsteady multidimensional simulations.

Key Words: dusty gas; shock wave; CFD; pseudo-stationary flows; parallel programming.

1. INTRODUCTION

The flow of a dusty gas, a gas containing a large number of small solid particles, is significantly different from that of a pure gas when the mass concentration of the particle is comparable to that of the pure gas. The difference is caused by the relaxation effects arising from the exchanges of momentum and heat between the gas and particles. The transition region in dusty gases typically is orders of magnitude thicker than that caused by viscosity and heat conduction in a pure gas and forms an example of nonequilibrium phenomena. Many researchers worked on the subject from many different aspects of the problem in

0021-9991/02 $35.00

1970s and 1980s. The shock wave propagation in a dusty gas is studied experimentally by the use of vertical shock tubes [12, 14, 18]. While various analytical and numerical techniques were developed to study how the shock wave structure changes with time in the dusty-gas shock tube. Otterman developed a numerical code adapting the particle-in-cell (PIC) method and investigated the dependence of numerical results on the models of drag and heat transfer between gas and particle phases [11]. In 1980s Miura and Glass created a one-dimensional numerical code using the random choice method (RCM) and published a series of papers [5–8] on their numerical and analytical results. Their numerical results show flow discontinuities without numerical diffusion, which is the unique feature of RCM. As a consequence, they could clearly distinguish a shock front from the nonequiliblium region behind it. Miura and Glass also carried out analytical studies on two-dimensional problems of supersonic steady flows in a dusty gas [9, 10]. In most analytical and numerical studies of the dusty-gas flows, solid particles are assumed to be perfect spheres with a constant diameter. This is only an approximation for shock-tube experiments. The assumption of uniform particle concentration is another assumption that is difficult to achieve in experiments. As a result, although comparisons among experimental, analytical and numerical studies were not so direct, the basic shock wave behavior in dusty gases, specially for one-dimensional problems, is quite well understood.

Recently, applications of dusty-gas flow studies to industrial and environmental issues have drawn attention. Serious studies for developing a system of removing dust particles from semiconductor wafers by using shock waves and nonstationary gasdynamic wave systems are examples of industrial applications [17]. The work of producing accurate hazard maps for volcanic eruptions is an important and urgent task since many people live quite close to active volcanos in Japan [21]. We have been working on producing hazard maps for these volcanos in Japan [15, 16]. Some of the volcanic disasters are strongly related to dusty-gas flows. The three-dimensional numerical simulations of dusty-gas flows with real terrain will provide us with much useful information in establishing better and more accurate safety measures.

The objective of the present study is to extend the previous work of Miura and Glass by developing a time-dependent multidimensional numerical code. The interactions between the gas and particle phases are calculated with the operator splitting technique. Therefore, we can choose numerical schemes for the different phases independently. In order to calculate the particle phase, we adapted a semi-analytical method combining the linear reconstruction of primitive variables in the numerical cell and an appropriate limiter for eliminating nonphysical numerical oscillations. All numerical results in this paper are obtained by using the Harten–Yee TVD scheme for the gas phase just because it is widely accepted and has been applied to many practical problems.

We constructed a vertical shock tube for carring out dusty-gas flow experiments at the Shock Wave Research Center (SWRC), Institute of Fluid Science, Tohoku University. This shock tube has a 1 m long observation window so that the whole relaxation region can be visualized at once. The experimental facility and the numerical code developed in the present study are useful tools in the investigation of complex shock wave phenomena in a dusty gas.

In what follows, a numerical code for simulating one-dimensional dusty-gas flows is introduced first. The results are compared with shock structures calculated from the pseudo-stationary analysis. The extension of the code to two-dimensional problems follows. The performance of a numerical code becomes increasingly important as the size of computation

becomes large. Throughout this study, computations are carried out on SGI Origin2000, a parallel computer with multiple RISC-based processors. The description of a parallel programing method, aimed at large three-dimensional calculations that are necessary for the aforementioned practical applications, is also provided. Discussions are made at appropriate places and a summary comes at the end.

2. NUMERICAL SCHEME OF ONE-DIMENSIONAL DUSTY-GAS FLOWS

In general, and also in this study, the following assumptions are made: (1) the gas follows the perfect-gas law; (2) the particles do not collide with each other so that they do not contribute to the pressure; (3) the shape of particles is spherical with a constant diameter; (4) the particles are inert; (5) the gravitational force is negligible; (6) the volume occupied by particles is negligible compared to that of gas; (7) the viscous and heat-conduction effects take place only between the gas and particles. In this section, the numerical method for calculating one-dimensional dusty-gas flows developed in the current study is described in detail.

2.1. Basic Equations

Under the previously made assumptions, the solid particles can be treated collectively as a continuum. Therefore, the dusty-gas flows are described by the conservation laws of mass, momentum, and total energy of both the gas and particles [8],

$$\frac{\partial \rho}{\partial t} + \frac{\partial}{\partial x}(\rho u) = 0, \tag{1}$$

$$\frac{\partial}{\partial t}(\rho u) + \frac{\partial}{\partial x}(\rho u^2 + p) = -\frac{\sigma}{m} D, \tag{2}$$

$$\frac{\partial E}{\partial t} + \frac{\partial}{\partial x}\{u(E + p)\} = -\frac{\sigma}{m}(u_d D + Q), \tag{3}$$

$$\frac{\partial \sigma}{\partial t} + \frac{\partial}{\partial x}(\sigma u_d) = 0, \tag{4}$$

$$\frac{\partial}{\partial t}(\sigma u_d) + \frac{\partial}{\partial x}\left(\sigma u_d^2\right) = \frac{\sigma}{m} D, \tag{5}$$

$$\frac{\partial \Omega}{\partial t} + \frac{\partial}{\partial x}(u_d \Omega) = \frac{\sigma}{m}(u_d D + Q), \tag{6}$$

where E and Ω are the total energies of the gas and particles, respectively, per unit volume and are expressed as

$$E = \rho\left(C_v T + \frac{1}{2}u^2\right), \quad \Omega = \sigma\left(C_m \Theta + \frac{1}{2}u_d^2\right).$$

The symbols ρ, p, T, u are the density, pressure, temperature, and flow velocity of the gas. The parameters of dust particles are denoted by the symbols σ, Θ, and u_d corresponding to the mass concentration, temperature, and velocity. Furthermore, m is the mass of a particle, D the drag force acting on a particle, and Q the rate of heat transfer to a particle. The symbols C_v and C_m are the specific heat of the gas at constant volume and the specific heat of the

solid particle, respectively. The thermally perfect equation of state for the gas is given by

$$p = \rho RT, \tag{7}$$

where R is the gas constant. The drag force D and the heat transfer rate Q are written in terms of the drag coefficient C_d and the Nusselt number N_u, which are expressed as

$$D = \frac{1}{8}\pi d^2 \rho (u - u_d)|u - u_d| C_d, \tag{8}$$

$$Q = \pi d \mu C_p P_r^{-1} (T - \Theta) N_u, \tag{9}$$

where d is the particle diameter and C_p is the specific heat of the gas at constant pressure. The drag coefficient and the Nusselt number depend on the particle Reynolds number, $\mathrm{R_e}$, as [1]

$$C_d = 0.46 + 28\mathrm{R_e}^{-0.85}, \tag{10}$$

and

$$N_u = 2.0 + 0.6 P_r^{\frac{1}{3}} \mathrm{R_e}^{\frac{1}{2}}. \tag{11}$$

The particle Reynolds number $\mathrm{R_e}$ is defined as

$$\mathrm{R_e} = \rho d|u - u_d|/\mu. \tag{12}$$

The viscosity and the thermal conductivity of the gas are assumed to vary only with the temperature. For air, that is used as the test gas in this paper, we assume the following formula taken from the reference [1]

$$\mu = 1.71 \times 10^{-5} (T/273)^{0.77} \quad \mathrm{N \times s/m^2}, \tag{13}$$

and the Prandtl number is assumed to be a constant,

$$P_r = 0.75. \tag{14}$$

2.2. Interaction between Gas and Particle Phases

The interaction between the gas and particles is caused by the drag and heat conduction between them, which is expressed as the inhomogeneous terms of the basic equations. In the present numerical code, the terms are treated separately from the flow calculations of the gas and dust particles using the operator splitting. At each time step, the following split equations

$$\frac{d}{dt}(\rho u) = -\frac{\sigma}{m} D, \tag{15}$$

$$\frac{dE}{dt} = -\frac{\sigma}{m}(u_d D + Q), \tag{16}$$

$$\frac{d}{dt}(\sigma u_d) = \frac{\sigma}{m} D, \tag{17}$$

$$\frac{d\Omega}{dt} = \frac{\sigma}{m}(u_d D + Q), \tag{18}$$

are solved in order to take the interactions into account. Then the flow calculations are carried out for the gas and dust particles independently solving homogeneous conservation equations that correspond to Eqs. (1) to (6). We tried several time integration schemes for Eqs. (15) to (18), such as the first-order Euler scheme and different orders of Runge–Kutta methods. We found no significant differences in the solutions among them, and decided to use the second-order Runge–Kutta method in order to be consistent with the accuracy of the numerical scheme for the gas and dust phases. It is worthwhile mentioning that, since the interaction between the gas and dust particles is included only in the inhomogeneous terms, the flow calculations for the gas and the dust particles are independent of each other. This enables us to develop numerical schemes separately for the two different phases, and we can try different combinations of them.

2.3. Flow Calculation of Gas Phase

The numerical code calculates the gas flow with a finite volume method. The numerical fluxes are obtained using the upwind TVD scheme of Harten [3] and Yee [22] together with Roe's approximate Riemann solver [13]. The scheme is second-order accurate both in space and time in the region where solutions are smooth. The numerical scheme is one of the most popular shock capturing schemes and its details are not repeated here. It is worthwhile mentioning, though, that the scheme has relatively high computational speed with reasonable robustness. This is important for multidimensional simulations of practical problems, especially for three-dimensional problems even with access to high performance computers.

2.4. Numerical Scheme for Dust Phase

We calculate the flow of the solid particles using a finite volume method that is consistent with the scheme used for the gas phase. The motion of dust particles is calculated conservatively by specifying the numerical fluxes of dust particles at the cell interfaces. Denoting the primitive dust parameters σ, u_d, and Θ symbolically by q, the initial data reconstruction between cell centers is made as

$$q(x, 0) = \frac{\Delta q}{\Delta x} x + q^{\mathrm{o}}, \tag{19}$$

where q^{o} is the value of q at the cell interface $x = 0$ at the beginning of each time step. As is usual for one-dimensional cases, if the cells are uniform, the value q^{o} is simply the average of cell values to the right and left of an interface. For nonuniform cells, denoting the distances from an interface to its left and right cell centers by dl and dr, respectively, it is given by the formula

$$q^{\mathrm{o}} = \frac{dr \times q_l + dl \times q_r}{\Delta x}, \quad \Delta x = dl + dr, \tag{20}$$

where q_l and q_r are the cell-center values of q to the left and right of a cell interface, respectively. With the linear interpolations of dust parameters Eq. (19), their values at the interface are explicitly obtained from the basic conservation equations Eqs. (4) to (6) in

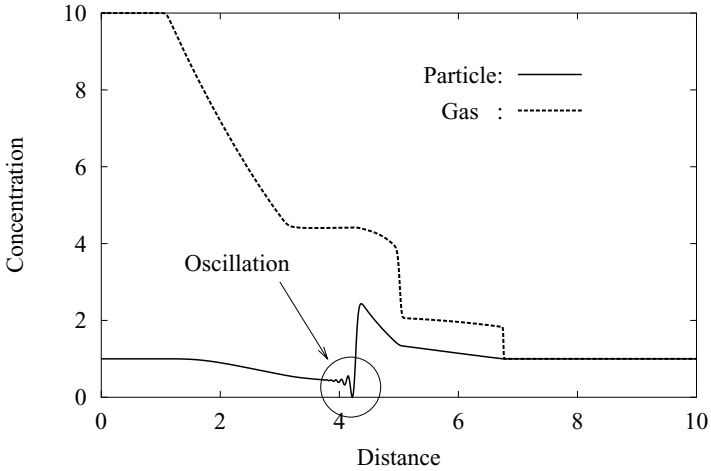

FIG. 1. Numerical instability in the dust–particle concentration.

terms of the gradients $\Delta u_d/\Delta x$, $\Delta\Theta/\Delta x$, and $\Delta\sigma/\Delta x$ as follows:

$$u_d = \frac{1}{1+\left(\frac{\Delta u_d}{\Delta x}\right)t}u_d^{\mathrm{o}}, \tag{21}$$

$$\Theta = \frac{1}{1+\left(\frac{\Delta u_d}{\Delta x}\right)t}\left[\left\{\left(\frac{\Delta u_d}{\Delta x}\right)\Theta^{\mathrm{o}} - \left(\frac{\Delta\Theta}{\Delta x}\right)u_d^{\mathrm{o}}\right\}t + \Theta^{\mathrm{o}}\right], \tag{22}$$

$$\sigma = \frac{1}{\left\{1+\left(\frac{\Delta u_d}{\Delta x}\right)t\right\}^2}\left[\left\{\left(\frac{\Delta u_d}{\Delta x}\right)\sigma^{\mathrm{o}} - \left(\frac{\Delta\sigma}{\Delta x}\right)u_d^{\mathrm{o}}\right\}t + \sigma^{\mathrm{o}}\right]. \tag{23}$$

The time averaged numerical fluxes at the cell interface are readily obtained by substituting the time t with one-half of the time step $\Delta t/2$.

The dust solutions calculated with this scheme alone are unstable. This is demonstrated in Fig. 1 with a dusty-gas shock tube problem. It is seen that the dust concentration oscillates in the region where its value changes rapidly as indicated by a circle in the figure. The oscillation grows in time and the solutions eventually diverge. This phenomena is similar to the instabilities observed in the gas phase solutions in the areas around large parameter changes when higher-order numerical schemes are used.

In this study, the instability is avoided by limiting the slopes of the reconstructed parameters that appear in Eqs. (21) to (23). We used the minmod function as the limiter that is expressed as

$$\Delta q = \Delta q_{i-\frac{1}{2}} \times \max\left(0, \min\left(1., \left(\Delta q_{i+\frac{1}{2}}\right)/\left(\Delta q_{i-\frac{1}{2}}\right)\right)\right), \tag{24}$$

where

$$\Delta q_{i+\frac{1}{2}} = q_{i+1} - q_i, \quad \Delta q_{i-\frac{1}{2}} = q_i - q_{i-1}.$$

As before, the symbol q represents any one of the dust parameters σ, u_d, or Θ. The nonphysical numerical oscillations do not appear with the slope limiter function. With the analogy to the numerical instability in pure-gas cases, we expect that the minmod limiter results in

TABLE I
Initial Conditions for Dusty-Gas Shock Tube Simulations

		Driver section	Driven section
Pressure	(p/p_{ref})	10.0	1.0
Gas density	(ρ/ρ_{ref})	10.0	1.0
Particle concentration	$(\sigma/\rho_{\text{ref}})$	0.0001	1.0
Gas velocity	(u/u_{ref})	0.0	0.0
Dust velocity	(u_d/u_{ref})	0.0	0.0

relatively smeared solutions but with higher stability. Although the investigation of other limiter functions, such as the superbee limiter function, is an interesting subject, we did not carry out further studies on the subject.

2.5. One-Dimensional Numerical Results and Discussions

A shock tube experiment with a dusty gas was simulated with the current numerical code. The initial conditions are listed in Table I. The gas in both the driver section and the driven section is air with $\gamma = 1.4$ at room temperature. The symbols p_{ref}, ρ_{ref}, and u_{ref} are the reference values. They are taken to be equal to the respective values for the initial state of the driven section (indicated by the subscript 1). It is also assumed that the ratio of specific heats of the two phases

$$\beta = C_m/C_v \tag{25}$$

is unity. Furthermore, we define the ratio of mass concentration in the reference state as

$$\alpha = \sigma_{\text{ref}}/\rho_{\text{ref}}. \tag{26}$$

In the present study, α is also assumed to be unity. The particle diameter d and the mass of a particle m are also important parameters for the numerical simulations and experiments. A characteristic quantity with the dimension of length, l, is deduced in the process of normalizing the basic equations as

$$l = \frac{8m}{\pi\rho_{\text{ref}}d^2} = \frac{3}{4}\frac{\sigma}{\rho_{\text{ref}}}d = \frac{3}{4}\frac{\sigma}{\rho_1}d. \tag{27}$$

We take l as the length scale and $\tau = l/u_{\text{ref}}$ as the time scale. Denoting the frozen speed of sound in the reference state as $a_{f,\text{ref}}$, the reference velocity is obtained as

$$u_{\text{ref}} = \frac{a_{f,\text{ref}}}{\sqrt{\gamma}} = \sqrt{\frac{p_{\text{ref}}}{\rho_{\text{ref}}}} = \sqrt{\frac{p_1}{\rho_1}}. \tag{28}$$

With this definition of reference velocity, we normalize the pressure and concentration of the gas and solid particles by p_1 and ρ_1.

The distributions of flow variables at five normalized time units after the diaphragm rupture ($\tau = 5$) are shown in Fig. 2. The plots of corresponding parameters for the pure-gas case with $\gamma = 1.4$ are also shown in the figure with thin solid lines for comparison.

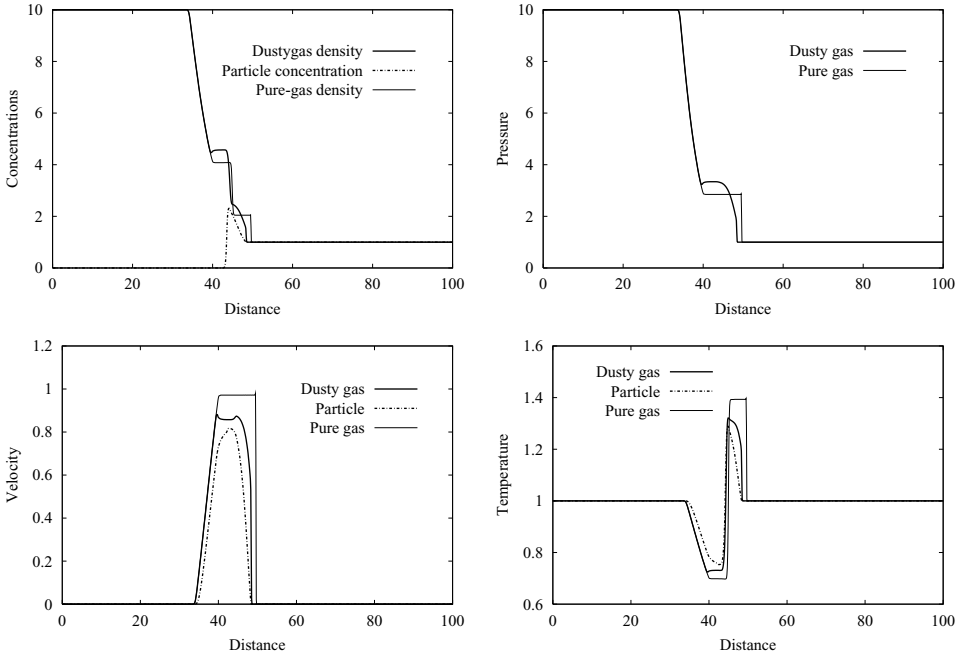

FIG. 2. Numerical results of dusty-gas shock tube problem at normalized time $\tau = 5$.

Usually, in experiments, dust particles are not introduced in the driver section. In the current study, however, an extremely small initial value is assigned for the value of particle concentration in the driver section, as shown in Table I. The value is so chosen that it is considered to be negligible compared with that in the driven section. The cell number is one thousand for the total tube length of 100 characteristic lengths, i.e., $\Delta x = 0.1$. The flux limiter for calculations of the gas phase is also the minmod function throughout this study.

Since particles cannot follow any abrupt changes due to large mass, the particle concentration slowly increases behind the frozen shock front until it reaches the maximum and then drops behind the contact surface. The effect of large particle inertia is also seen in the velocity profile. It is known that the shock waves in dusty gases can be either fully dispersed or partially dispersed depending on whether the propagation speed of the shock wave exceeds the frozen speed of sound [7, 8]. The present case is in the partially dispersed shock wave regime. The shock profiles in the gas consists of a sharp frozen shock wave front that appear as abrupt parameter changes and a region where those parameters gradually increase. The gas loses energy due to interactions with particles and the shock front is decelerated. This is noticeable in the figure by comparing the shock wave position with that for the pure gas. The deceleration of the shock wave front induces compression waves behind the shock front and the pressure increases to a higher value than that of the pure-gas case. The rarefaction wave, as a result, is reduced and the temperature does not decrease so much as in the pure-gas case. At the time $\tau = 5$, the gas and particles have not yet reached equilibrium. The numerical results at later times $\tau = 10$ and $\tau = 30$ are shown in Figs. 3 and 4, respectively. It is seen from the velocity and temperature profiles in Fig. 3 that the two phases become almost in equilibrium at the contact surface. The fully developed equilibrium regions are seen in Fig. 4.

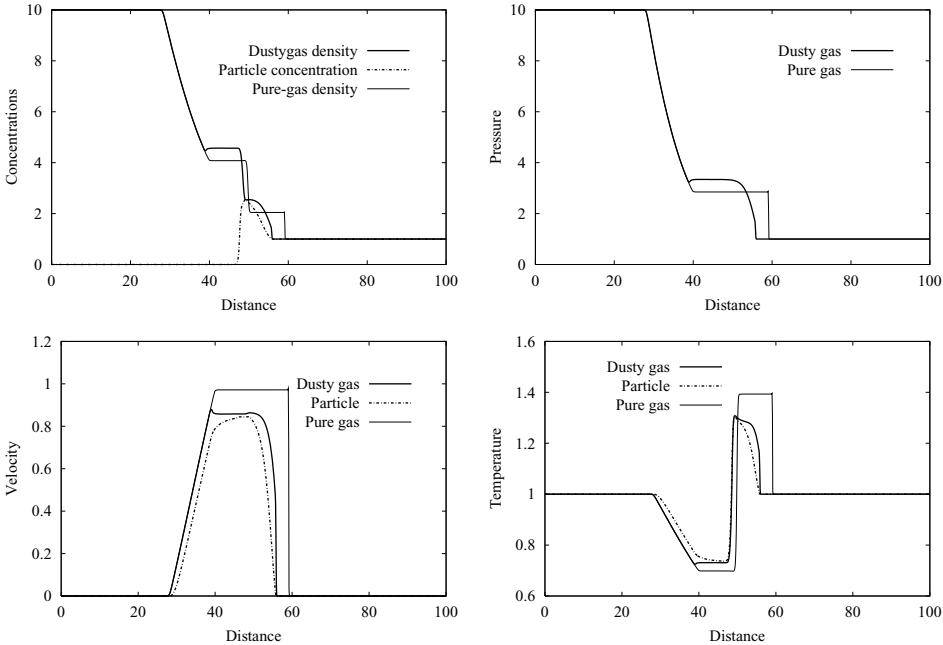

FIG. 3. Numerical results of dusty-gas shock tube problem at normalized time $\tau = 10$.

2.6. Pseudo-stationary Analysis

After the two phases become in equilibrium, the shock wave velocity becomes constant. Then the transition region, behind the shock front to the equilibrium region, becomes the

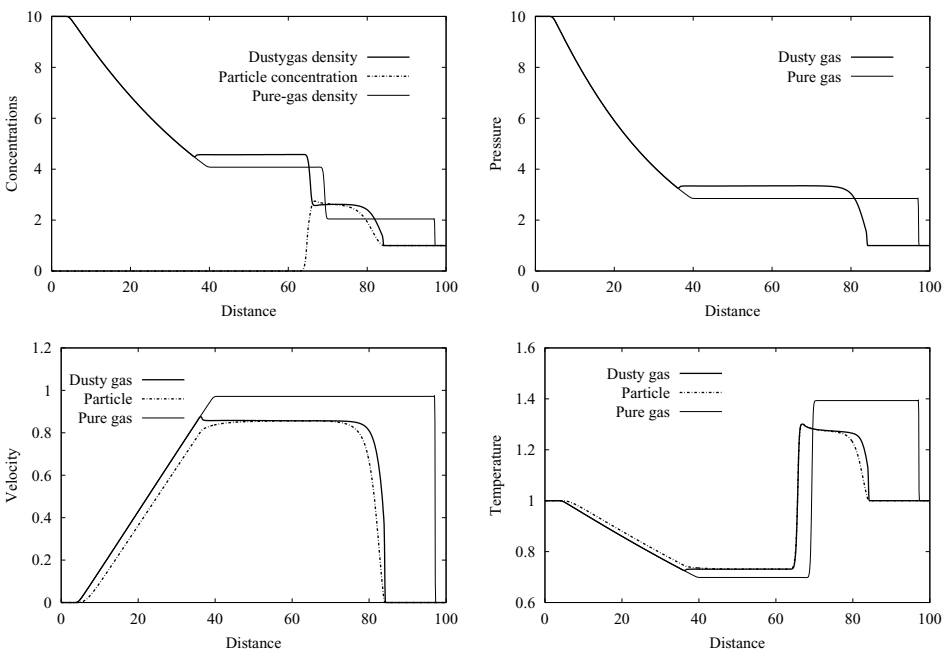

FIG. 4. Numerical results of dusty-gas shock tube problem at normalized time $\tau = 30$.

pseudo-stationary solution. Here, the numerically obtained shock structures with the current numerical code are compared with the analytically obtained pseudo-stationary solutions as one of the code validations. The time-dependent basic equations for conservation laws, Eqs. (1) to (6), become, after Galilean transformation and some manipulations, the following form:

$$\frac{d}{dx}(\rho u) = 0, \tag{29}$$

$$\frac{d}{dx}(\sigma u_d) = 0, \tag{30}$$

$$\frac{d}{dx}\left(\rho u^2 + \sigma u_d^2 + p\right) = 0, \tag{31}$$

$$\frac{d}{dx}\left(\rho u\left(C_p T + \frac{1}{2}u^2\right) + \sigma v\left(C_m \Theta + \frac{1}{2}u_d^2\right)\right) = 0, \tag{32}$$

$$\frac{du_d}{dx} = \frac{D}{mu_d}, \tag{33}$$

$$\frac{d\Theta}{dx} = \frac{Q}{mC_m u_d}. \tag{34}$$

Integrating these equations together with the equation of state, Eq. (7), we obtain the pseudo-stationary shock wave profiles. Any standard numerical method would do the numerical integration and, here, we used the fourth-order Runge–Kutta method. The numerical results obtained by the numerical code developed in the previous sections are compared with the pseudo-steady solutions in Fig. 5.

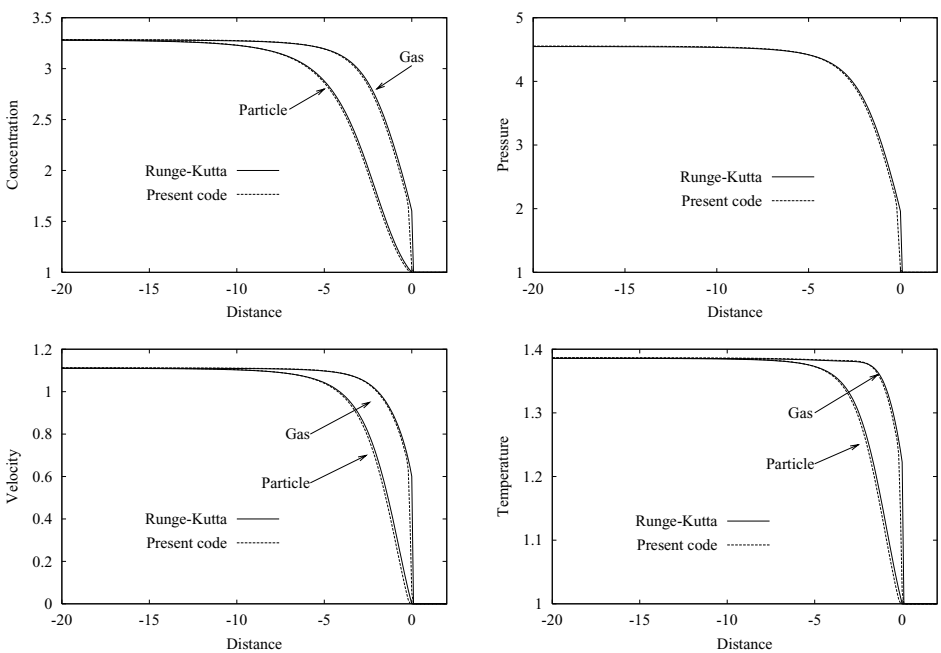

FIG. 5. Comparison of shock wave structure: Results from the current time-dependent numerical code (broken lines); pseudo-stationary solutions (solid lines).

The comparison was made for the shock wave with the propagation speed of Mach 1.35, which is obtained in the dusty-gas shock tube with the same initial conditions as the previous shock tube case except the pressure and density ratios increased to 20. The agreement of the profiles calculated with present numerical code with pseudo-stationary solutions is quite good.

Figures 3 to 5 also provide us with useful information about the size of the nonequilibrium region. It is found that the region extends about 15 times the characteristic length l. If crown glass (2,500 kg/m^3) particles of 10 μm diameter are used, the characteristic length becomes 2.7 cm and the nonequilibrium region extends about 40 cm behind the frozen shock front.

3. EXTENSION TO MULTIDIMENSIONAL FLOWS

The extension of the one-dimensional code described in the previous sections to multidimensional flow problems is straightforward. Here we describe it for two-dimensional (2D) case. The code optimization is also considered since it is an important issue for large-scale multidimensional calculations.

3.1. Basic Equations

The basic equations for two-dimensional flows are

$$\frac{\partial \rho}{\partial t} + \frac{\partial}{\partial x}(\rho u) + \frac{\partial}{\partial y}(\rho v) = 0, \tag{35}$$

$$\frac{\partial}{\partial t}(\rho u) + \frac{\partial}{\partial x}(\rho u^2 + p) + \frac{\partial}{\partial y}(\rho u v) = -\frac{\sigma}{m} D_x, \tag{36}$$

$$\frac{\partial}{\partial t}(\rho v) + \frac{\partial}{\partial x}(\rho u v) + \frac{\partial}{\partial y}(\rho v^2 + p) = -\frac{\sigma}{m} D_y, \tag{37}$$

$$\frac{\partial E}{\partial t} + \frac{\partial}{\partial x}\{u(E + p)\} + \frac{\partial}{\partial y}\{v(E + p)\} = -\frac{\sigma}{m}(u_d D_x + v_d D_y + Q), \tag{38}$$

$$\frac{\partial \sigma}{\partial t} + \frac{\partial}{\partial x}(\sigma u_d) + \frac{\partial}{\partial y}(\sigma v_d) = 0, \tag{39}$$

$$\frac{\partial}{\partial t}(\sigma u_d) + \frac{\partial}{\partial x}\left(\sigma u_d^2\right) + \frac{\partial}{\partial y}(\sigma u_d v_d) = \frac{\sigma}{m} D_x, \tag{40}$$

$$\frac{\partial}{\partial t}(\sigma v_d) + \frac{\partial}{\partial x}(\sigma u_d v_d) + \frac{\partial}{\partial y}\left(\sigma v_d^2\right) = \frac{\sigma}{m} D_y, \tag{41}$$

$$\frac{\partial \Omega}{\partial t} + \frac{\partial}{\partial x}(u_d \Omega) + \frac{\partial}{\partial y}(v_d \Omega) = \frac{\sigma}{m}(u_d D_x + v_d D_y + Q), \tag{42}$$

where E and Ω are again the total energies per unit volume for the gas and particles, respectively, and for two-dimensional flows, expressed as

$$E = \rho\left\{C_v T + \frac{1}{2}(u^2 + v^2)\right\}, \quad \Omega = \sigma\left\{C_m \Theta + \frac{1}{2}\left(u_d^2 + v_d^2\right)\right\}.$$

The symbols v and v_d are the velocities of the gas and dust particles, respectively, in the y-direction. Furthermore, D_x and D_y are the drag-force elements acting on a particle in the

x- and y-directions given as

$$D_x = \frac{1}{8}\pi d^2 \rho (u - u_d)|u - u_d| C_d, \quad D_y = \frac{1}{8}\pi d^2 \rho (v - v_d)|v - v_d| C_d. \tag{43}$$

Notions of other parameters are the same for the one-dimensional case. The thermally perfect equation of state for the gas is already given in Eq. (7). Corresponding to the extention, the expression of Nusselt number is unchanged but the particle Reynolds number is modified to

$$\mathrm{R_e} = \rho d \sqrt{(u - u_d)^2 + (v - v_d)^2}/\mu. \tag{44}$$

3.2. Strategy of Extension to Multidimensional Flows

Strang type operator splitting [19] is widely used for extending the one-dimensional code to multidimensional one. We use the method for calculating the set of homogeneous equations corresponding to the basic equations Eqs. (35) to (42) both for the gas and particle phases. As in one-dimensional code, the inhomogeneous terms representing the effects of drag and heat conduction are also treated by operator splitting. The operator splitting is a well-accepted numerical technique and is described in [20], for example.

3.3. Numerical Scheme for Particle Flows

The distribution functions of dust parameters are defined in the same way as in the one-dimensional case,

$$q(s, 0) = \frac{\Delta q}{\Delta s} s + q^{\mathrm{o}}, \tag{45}$$

where s is the distance measured in the normal direction of a cell interface for which the numerical fluxes are evaluated. The term q^{o} is the initial value of q at $s = 0$ and is expressed as

$$q^{\mathrm{o}} = \frac{dr \times q_l + dl \times q_r}{\Delta s}, \quad \Delta s = dl + dr. \tag{46}$$

When we substitute these into the basic equations Eqs. (39) to (42), the expressions result for the solutions at the cell interface

$$\tilde{u}_d = \frac{1}{1 + \left(\frac{\Delta \tilde{u}_d}{\Delta s}\right) t} \tilde{u}_d^{\mathrm{o}}, \tag{47}$$

$$\tilde{v}_d = \frac{1}{1 + \left(\frac{\Delta \tilde{u}_d}{\Delta s}\right) t} \left[\left\{ \left(\frac{\Delta \tilde{u}_d}{\Delta s} \right) \tilde{v}_d^{\mathrm{o}} - \left(\frac{\Delta \tilde{v}_d}{\Delta s} \right) \tilde{u}_d^{\mathrm{o}} \right\} t + \tilde{v}_d^{\mathrm{o}} \right], \tag{48}$$

$$\Theta_d = \frac{1}{1 + \left(\frac{\Delta \tilde{u}_d}{\Delta s}\right) t} \left[\left\{ \left(\frac{\Delta \tilde{u}_d}{\Delta s} \right) \Theta_d^{\mathrm{o}} - \left(\frac{\Delta \Theta_d}{\Delta s} \right) \tilde{u}_d^{\mathrm{o}} \right\} t + \Theta_d^{\mathrm{o}} \right], \tag{49}$$

$$\sigma_d = \frac{1}{\left\{1 + \left(\frac{\Delta \tilde{u}_d}{\Delta s}\right) t\right\}^2} \left[\left\{ \left(\frac{\Delta \tilde{u}_d}{\Delta s} \right) \sigma_d^{\mathrm{o}} - \left(\frac{\Delta \sigma_d}{\Delta s} \right) \tilde{u}_d^{\mathrm{o}} \right\} t + \sigma_d^{\mathrm{o}} \right], \tag{50}$$

where $\tilde{u}_d$ and $\tilde{v}_d$ are the velocity components of particles in the normal and tangential directions to the cell interface. Time averaged numerical fluxes over the time step can be

calculated from these solutions by putting $\Delta t/2$ into t. The slope limiters as in Eq. (20) are implemented in order to suppress the numerical instabilities.

3.4. Code Optimizations

There are several ways of parallelizing the code on SGI Origin2000. The most simple programming is the shared-memory based programming of OpenMP [24]. With this method, we parallelize DO loops (for FORTRAN) just as we vectorize them using directives. With OpenMP, however, optimizations for single-CPU performance and for parallel performance sometimes conflict with each other. Namely, a code modification made for increasing the single-CPU performance often makes the scalability between computational speed and the number of CPUs used for the program execution worse. Therefore, the performance as a whole is hard to control.

In the present study, we use MPI (message passing interface) [23] together with domain decomposition. MPI is based on the distributed-memory concept and the code is free from cache false sharing, one of the most severe factors that degrade the scalability in parallel computations. As a result, the scalability of the code is independent of the single-CPU performance. Therefore, we have better control on the code performance with MPI.

In the program, the global computational area is first divided into the same number of subdomains as the prescribed number of CPUs. Each CPU then reads the data of its corresponding subdomain and carries out calculations by communicating with neighboring CPUs using MPI library calls.

3.5. Numerical Example

A simple problem of explosion of a square column filled with pressurized dusty gas was calculated. The initial filling pressure and gas density are both 10 times greater than the corresponding values outside the column. The initial mass concentration of particles is also 10 times greater than the gas density outside the column. The physical properties of the gas and particles are taken to be the same as those used for the one-dimensional calculations in the previous sections. The numerical results of particle-concentration distributions at two different moments $\tau = 2$ and 5, together with the initial distribution, are shown in Fig. 6. Although quantitative validations are not made due to lack of experimental data, it is demonstrated how the particles spread out into the surrounding space. No numerical instability was observed during the computation, and the numerical results shown in Fig. 6 keep symmetry quite well. Since this is only a sample test problem, the calculation was carried out using a small number of 128×128 numerical cells. The execution time on the SGI Origin2000 is 25 seconds with one CPU and 5.7 seconds with eight CPUs for calculating 70 time steps corresponding to $\tau = 6$. The average speed per CPU is 99 Mflops for single-CPU execution and 88 Mflops for eight-CPU execution. Considering the fact that the program size is relatively small for eight CPUs to work on, the code performance is satisfactory. For larger problem size, the relative execution time for the serial part of the program as well as for the inter CPU communications to that of net flow calculation decreases and, as a result, both the CPU speed and the scalability of parallel execution increases.

It is known that the dust-phase equations have an deficiency associated with the assumption that dust particles do not collide with each other. Due to this assumption, no

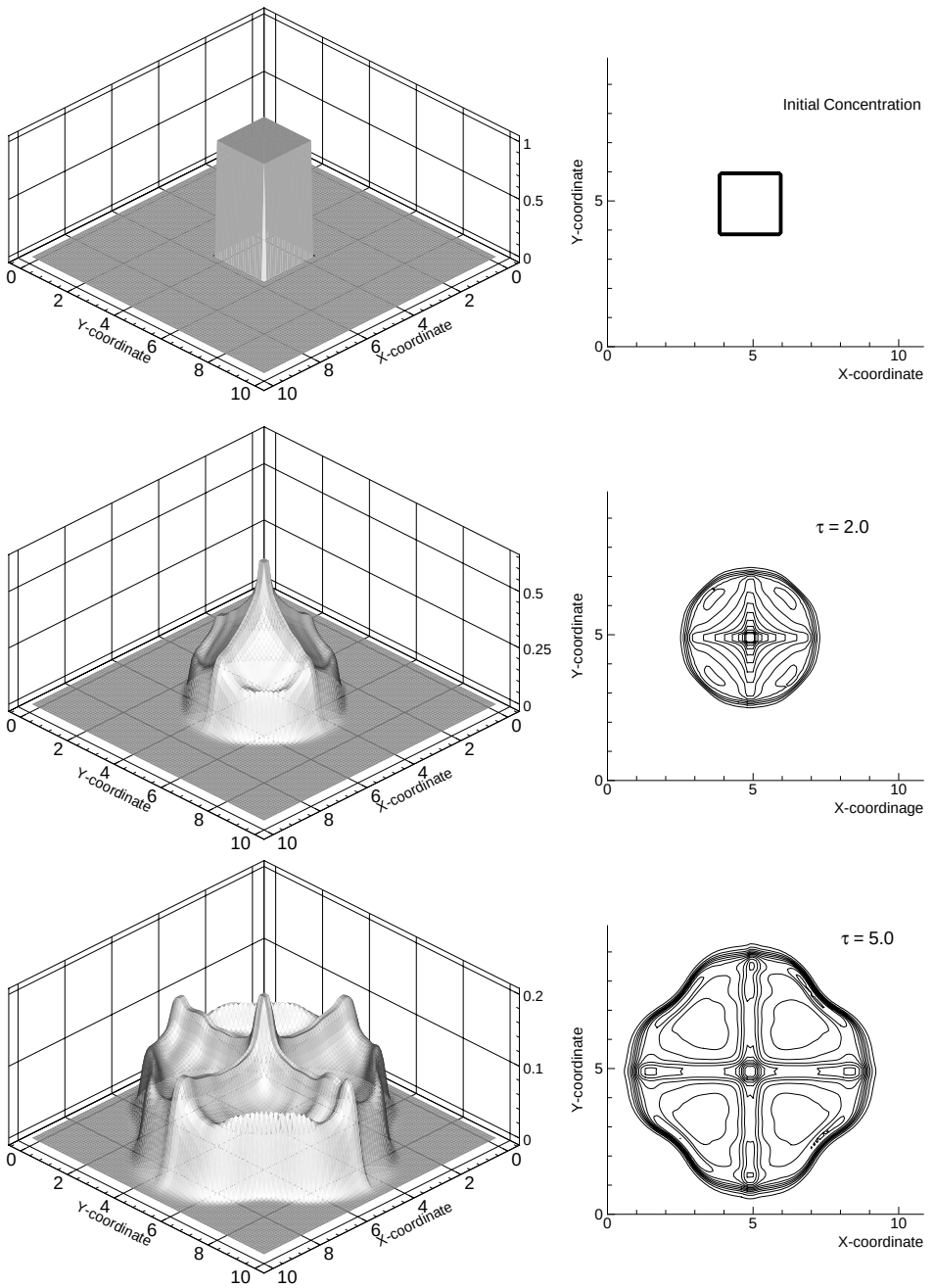

FIG. 6. Dust particle concentration of explosion of pressurized square column filled with dusty gas: initial dust concentration (top); $\tau = 2.0$ (middle); $\tau = 5.0$ (bottom).

restoring force acts among dust particles and the particle concentration may increase to an unrealistically high value in a converging velocity field. This could be observed, for example, near the wedge surface when oblique shock wave reflections are simulated. When the particle concentration becomes too high, another basic assumption of neglecting the particle volume becomes invalid. It is, therefore, important to be aware of the significance of the

underlying assumptions and their consequences. Works for improving the code by replacing the assumptions described in Section 2 by reasonable mathematical models are now being carried out. We have constructed a vertical dusty-gas shock tube at SWRC. It has a 100×150 mm cross section and an observation window of 1 m long, so that the whole nonequilibrium region can be visualized for each experiment. A variety of dusty-gas flow problems are planned to be investigated using the present numerical code and the experimental facility in order to construct and validate the mathematical models to improve the numerical code.

SUMMARY

A numerical code for calculating shock wave propagations in dusty gases is developed. The numerical solutions for one-dimensional case is validated with pseudo-stationary solutions. It is found that the nonequilibrium region extends about 15 times the characteristic length. The numerical code is extended to two-dimensional flow problems using MPI and the domain decomposition. The numerical code has satisfactory execution speed and scalability for parallel computations.

REFERENCES

1. S. Chapman and T. G. Cowling, *The Mathematical Theory of Non-Uniform Gases* (Cambridge University Press, Cambridge, UK, 1961).
2. M. Gilbert, L. Davis, and D. Altman, Velocity lag of particles in linearly accelerated combustion gases, *Jet Propulsion* **25**, 26 (1955).
3. A. Harten, High resolution schemes for hyperbolic conservation laws, *J. Comput. Phys*. **49**, 357 (1983).
4. J. G. Knudsen and D. L. Katz, *Fluid Mechanics and Heat Transfer* (McGraw–Hill, New York, 1958).
5. H. Miura and I. I. Glass, On a dusty-gas shock tube, *Proc. R. Soc. Lond. A* **382**, 373 (1982).
6. H. Miura and I. I. Glass, On the passage of a shock wave through a dusty-gas layer, *Proc. R. Soc. Lond. A* **385**, 85 (1983).
7. H. Miura and I. I. Glass, Development of the flow induced by a piston moving impulsively in a dusty gas, *Proc. R. Soc. Lond. A* **397**, 295 (1985).
8. H. Miura, T. Saito, and I. I. Glass, Shock-wave reflection from a rigid wall in a dusty gas, *Proc. R. Soc. Lond. A* **404**, 55 (1986).
9. H. Miura and I. I. Glass, Oblique shock waves in a dusty-gas flow over a wedge, *Proc. R. Soc. Lond. A* **408**, 61 (1986).
10. H. Miura and I. I. Glass, Supersonic expansion of a dusty gas around a sharp corner, *Proc. R. Soc. Lond. A* **415**, 91 (1988).
11. B. Otterman and A. S. Levine, Analysis of gas–solid particle flows in shock tubes, *AIAA J.* **12**(5), 579 (1974).
12. E. Outa, K. Tajima, and H. Morii, Experiments and analyses on shock waves propagating through a gas–particle mixture, *Bull. JSME* **19**(130), 384 (1976).
13. P. L. Roe, Approximate Riemann solvers, parameter vectors, and difference schemes, *J. Comput. Phys*. **43**, 357 (1981).
14. G. Rudinger, Effective drag coefficient for gas–particle flow in shock tubes, *Trans. Am. Soc. Mech. Eng, J. bas. Eng. D* **92**, 165 (1970).
15. T. Saito, T. Eguchi, K. Takayama, and H. Taniguchi, Hazard predictions for volcanic explosion, *J. Volcanology Geothermal Res.* **106**, 39 (2001).
16. T. Saito, T. Kitamura, K. Takayama, H. Fujii, and H. Taniguchi, Numerical simulation of blast wave propagation induced by eruptions of volcanoes, *Shock Waves, Proc. 19th ISSW* **III**, 385 (1994).

17. K. Shibasaki, S. Shibasaki, G. Jagadeesh, M. Sun, and K. Takayama, Development of a high-speed cylindrical rotor device for industrial applications of shock waves, in *Proc. 23rd. Int. Symposium on Shock Waves, July 2001*, edited by F. Lu, to appear.
18. M. Sommerfeld and H. Grönig, Decay of shock waves in a dusty-gas shock tube with different configurations, in *Proc. 14th International Symposium on Shock Tubes and Waves*, edited by F. D. Archer and B. E. Milton (Sydney Shock Tube Symposium Publishers, 1984), pp. 470–477.
19. G. Strang, On the construction and comparison of difference schemes, *SIAM J. Numer. Anal*. **5**(3), 506 (1968).
20. E. F. Toro, *Riemann Solvers and Numerical Methods for Fluid Dynamics* (Springer-Verlag, Heidelberg, 1997).
21. T. Ui, *Volcanic Eruptions and Disasters* (Tokyo Univ. Press, Tokyo, 1997).
22. H. C. Yee, Upwind and symmetric shock-capturing schemes, NASA TM 89464 (1987).
23. http://www.mpi-forum.org/docs
24. http://www.openmp.org/openmp